OPEN ACCESS

Matter wave optics perspective at molecular photoionization: K-shell photoionization and Auger decay of N_2

New Journal of Physics
The open-access journal for physics

Matter wave optics perspective at molecular photoionization: K-shell photoionization and Auger decay of N_2

M S Schöffler[1,2,5], T Jahnke[1], J Titze[1], N Petridis[1], K Cole[1], L Ph H Schmidt[1], A Czasch[1], O Jagutzki[1], J B Williams[3], C L Cocke[4], T Osipov[2], S Lee[2], M H Prior[2], A Belkacem[2], A L Landers[3], H Schmidt-Böcking[1], R Dörner[1] and Th Weber[2]

[1] Institut für Kernphysik, University Frankfurt, Max-von-Laue-Strasse 1, 60438 Frankfurt, Germany
[2] Lawrence Berkeley National Laboratory, Berkeley, CA 94720, USA
[3] Department of Physics, Auburn University, Auburn, AL 36849, USA
[4] Department of Physics, Kansas State University, Cardwell Hall, Manhattan, KS 66506, USA
E-mail: schoeffler@atom.uni-frankfurt.de

New Journal of Physics **13** (2011) 095013 (14pp)
Received 5 April 2011
Published 20 September 2011
Online at http://www.njp.org/
doi:10.1088/1367-2630/13/9/095013

Abstract. In this paper, we shed new light on the molecular photoionization of a diatomic molecule. We will elaborate the differences and analogy between a quantum optical and light–matter interaction approach in a study of K-shell photoionization of N_2 in which the photoelectron and the subsequently emitted Auger electron are both measured in coincidence in the body fixed frame of the molecule. The two electrons form an entangled state inside a double slit. By changing the photon energy we create different types of interference in the photoelectron and the Auger electron wave.

[5] Author to whom any correspondence should be addressed.

Contents

1. Introduction

Ejection of an electron from a tightly bound 1s orbital by photoabsorption is a convenient way to create an extremely well-controlled electron wave. The wavelength of that wave can be tuned by changing the photon energy. The initial photoelectron wave is not spherical but has an angular distribution imprinted on it, which is imposed by the photon angular momentum. The wavelength changes as the electron escapes from the Coulomb potential. If the 1s electrons that absorbed the photon are part of a molecule or a crystal, these photoelectron waves can be used for many fascinating matter wave experiments showing two different types of interference effects [1]. Firstly, the electron wave can be multiply scattered at neighboring centers in the molecule. This interference will be observed as a function of the photoelectron wavelength at a fixed ejection angle or as strong oscillations of the electron flux depending on the emission angle of the electron with respect to the molecular axis. These oscillations in the total absorption cross section [2] are well understood and are frequently used to actually measure the distances and locations of the nearest scattering centers in extended x-ray absorption fine structure (EXAFs) [3]. X-ray photoelectron diffraction (XPD) makes additional use of the emission angle dependence [4]. For molecules in the gas phase they can be used to 'illuminate the molecule from within' [5]. In the most advanced experiments, circularly polarized light is used, which allows us to obtain a stereoscopic picture of the neighbors in such electron diffraction patterns [6]. When the electron wavelength is comparable to the bond length, multiple scattering of the electron can result in quasi-standing waves in the multicenter potential of the molecule, which give rise to the so-called shape resonances. They manifest themselves in a resonant enhancement of the photoionization cross section and a highly structured angular distribution of the photoelectron [7, 8]. As expected, these features show a strong dependence on the internuclear distance [9–13] and are usually strong for the sigma-shape resonance.

Secondly, in a homonuclear molecule the initial photoelectron wave will emerge coherently from two indistinguishable centers. This resembles the situation of a double-slit experiment [14–16]. For the hydrogen molecule, this has been shown for photoionization [17–19] and for ion impact [20–22] and has also been predicted for strong field ionization [23–25]. These studies confirmed the dependence of the interference pattern on the internuclear distance of the two centers [26] as well as on the electron wavelength [18].

For all other homonuclear diatomics but H_2, the situation is slightly more complicated, since the two K-shells are fully filled with a total of four electrons. This situation is described by using a molecular basis of a gerade state, which is the sum of two orbitals being located at either atom of the molecule, i.e. the sum of the contribution of the 'left' atom and the 'right' atom of the molecule. The ungerade molecular state in turn is the difference of these two contributions.

Ejection from the gerade state is the analogue of a classical double-slit experiment, as the two waves emerge in phase, while emission from the ungerade state corresponds to a double-slit experiment with a π phase shifter in one of the slits. This leads to the conversion of interference maxima to minima. Note that the ground state of the N_2 molecule is a gerade state. The intermediate state after core hole creation of N_2^+ can be either of gerade or ungerade parity. Hence, any experiment that does not distinguish between core holes in gerade or ungerade orbitals will not see an interference pattern since the maxima and minima cancel out. The gerade and ungerade levels are slightly shifted in energy (about 100 meV in N_2 [27]). If this energy splitting is larger than the natural line width, given by the core hole lifetime, the symmetry of the state can in principle be resolved. An experiment with sufficient energy resolution will then observe the analogue to fringes and anti-fringes observed in optical double-slit experiments in the electron angular distribution of the gerade or ungerade state, respectively. If, in contrast, the natural line width is bigger than the gerade–ungerade energy splitting, the interference cannot be resolved by just detecting the photoelectron. However, it turns out that by coincident detection with the Auger electron, the interference can be restored if in addition the symmetry of the N_2^{2+} ion in the final state is measured. We will discuss this point in more detail below.

All K holes in N_2 can decay by emission of an Auger electron. In this case, an outershell electron fills the hole and another outershell electron is emitted to the continuum. As the outershell orbitals are typically not localized, one might at first glance expect that these Auger electrons do not show any two-center interference. This picture, however, neglects the nature of the Auger effect. In the Auger decay the energy needs to be transferred to the ejected electron via Coulomb interaction between the electron that filled the hole and the emitted outershell electron. This strong Coulomb interaction requires that the two electrons be spatially close and both in the vicinity of the hole. In the Coulomb matrix element, this becomes obvious by the $1/r_{12}$ term, where r_{12} is the distance of the two interacting electrons. As a consequence, two-center interference in Auger electron angular distributions has been predicted in [13] and seen in the experiments. These experiments have also shown that the interference fringes on the Auger electron angular distribution depend on the internuclear distance, as expected from a double slit.

The emitted Auger electrons also show the same two interference effects as the photoelectron discussed above. There might be a π-phase shift between the Auger electron waves from the two centers. This depends on the parity of the hole, as well as on the parity of the electron that fills the hole and the one that is emitted. Furthermore, the Auger electrons experience the same multiple scattering in the molecular potential as the photoelectrons, giving rise to additional interferences from the wave scattered at the neighboring nuclei.

So far, we have discussed the emission of the photoelectron and the Auger electron as two independent steps. This is not correct however, since the Auger electron is emitted in a process that fills the hole from which the photoelectron was emitted earlier. In addition to this obvious link in symmetry, the photoelectron and the Auger electron also interact in the continuum and there has been a dispute over whether there is a memory of the photon absorption in the molecule in addition to the site from which it was emitted [28–30], which was called the 'breakdown of the two-step model' and its 'resurrection'. These latter effects are not central in the current context. The link via the intermediate core hole state, however, is of central importance. The intermediate core hole state entangles both electrons as we have shown in [31].

In the previous work [31], we investigated the reaction:

$$419\,\mathrm{eV}h\nu + \mathrm{N_2} \rightarrow e_{\mathrm{photo}}(10\,\mathrm{eV}) + e_{\mathrm{Auger}} + \mathrm{N^+} + \mathrm{N^+}. \quad (1)$$

We have detected the kinetic energy and emission angle of all four particles. From the direction of the two ions, we obtain the molecular axis at the instant of photoabsorption. The N_2^{2+} ion, which finally dissociates to $N^+ + N^+$, can either be in a state of gerade or ungerade parity. As we will address the parity of the Auger and photoelectron pairs, it is essential that the parity of the final N_2^{2+} state be known. Luckily, in the case of dissociating N_2^{2+}, there are regions of the kinetic energy release (KER) of the $N^+ + N^+$ which are related to intermediate N_2^{2+} of well-defined parity. We are therefore able to deduce the parity of ions in the N_2^{2+} final state [13, 32, 33] from the measured KER. For a fixed direction of the molecular axis and a well-defined parity of the N_2^{2+} state, we then studied the correlation between the photoelectron and the Auger electron emission angle. They can successfully be described by considering the two electrons in an entangled state, very similar to a Bell state. The cross section for coincident detection of a photoelectron into the solid angle element $d\Omega_{\vec{k}_p}$ and an Auger electron into $d\Omega_{\vec{k}_a}$ is given by

$$\frac{d\sigma}{d\Omega_{\vec{k}_a} d\Omega_{\vec{k}_p}} = \sum_f |\langle \Psi_f^{++} \psi_{\vec{k}_a}^- | V | \Psi_{\sigma_g}^+ \rangle \langle \Psi_{\sigma_g}^+ \psi_{\vec{k}_p}^- | d | \Psi_0 \rangle + \langle \Psi_f^{++} \psi_{\vec{k}_a}^- | V | \Psi_{\sigma_u}^+ \rangle \langle \Psi_{\sigma_u}^+ \psi_{\vec{k}_p}^- | d | \Psi_0 \rangle|^2. \quad (2)$$

Here, $\langle \Psi_{1\sigma_{g,u}}^+ \psi_{\vec{k}_p}^- | d | \Psi_0 \rangle$ is the dipole amplitude describing the photoelectron emission and $\langle \Psi_f^{++} \psi_{\vec{k}_a}^- | V | \Psi_{1\sigma_{g,u}}^+ \rangle$ is the matrix element describing the Auger emission. The key here is that the emission via the gerade and ungerade molecular states $\Psi_{1\sigma_{g,u}}^+$ for the intermediate, core-ionized singly charged ion is added coherently, resulting in an entanglement between the two electrons.

The purpose of the present paper is to explore the interplay of the entanglement of the photo- and Auger electron and the interference effects from the scattering at the molecular centers in some more detail. This extends our previous study [31] as we altered the photoelectron wavelength by changing the photon energy. A change of the photon energy does not directly affect the Auger decay or intermediate core hole state. It does, however, change the interference originating from the scattering of the photoelectron strongly, as we will show below.

2. Experiment

We performed the experiment at the Advanced Light Source of the Lawrence Berkeley National Laboratory using circularly polarized photons provided by the beamline 11.0.2, by applying the cold target recoil ion momentum spectroscopy (COLTRIMS) method [34–36]. In the experiment, we detected the vector momenta of the slow photoelectron and the two N^+ ions directly; the momentum vector of the fast Auger electron was deduced by incorporating momentum conservation. To achieve a maximum resolution the gas for the supersonic beam was precooled to 130 K. This reduced both the jet velocity and the momentum spread in the longitudinal direction of the jet (expansion direction). Furthermore, we used a high driving pressure of 20 bar to reach a high speed ratio, i.e. a minimal momentum spread of the gas target (1.7 a.u. estimated from the experiment).

We used a weak electric field (varying 12–18 V cm^{-1}) to project the electrons and ions onto position and time-sensitive multichannel plate detectors (80 mm diameter) equipped with delay line anodes for position readout [37]. As the photoelectrons are much lighter than the ions and have a high velocity, they tend to escape the spectrometer. Therefore a magnetic field (6.5–15 G) was superimposed in parallel to the electric field to guide the electrons toward the electron detector [38]. This technique of catching fast electrons is usually limited to electron energies

below 100 eV, as energy and angular resolution decrease with increasing electromagnetic field strength.

The experiment requires us to measure a low energetic photoelectron (5, 10, 18 and 56 eV) in coincidence with a much higher energetic Auger electron (370 eV) and the two ionic fragments (∼5 eV per ion). Typical COLTRIMS approaches for molecular fragmentation studies so far employed short ion arms on the spectrometer in order to achieve a solid angle of detection of 4π for the ions as described in [36]. In the present case, we adopted a spectrometer geometry usually used for investigations of atoms [39]. In that approach, time and space focusing is used in order to maximize the momentum resolution of the measured ion. For molecular targets the ionic fragments typically undergo Coulomb explosion, resulting in high kinetic energies. Therefore the resulting long spectrometer and the low electric field reduced the total acceptance angle. The momentum resolution, on the other hand, is dramatically increased. The 3D focusing geometry of the recoil ion spectrometer allowed us to get rid of the diminishing influence of the size of the interaction region. The use of an electrostatic lens in the acceleration region improved the resolution at least by a factor of 3. From the non-dissociating doubly charged N_2^{2+} ion channel, we extracted an overall momentum resolution for the Auger electron of 1.8 a.u. in the jet, 0.45 a.u. in the photon beam and 0.4 a.u. in the time-of-flight (TOF) direction. For the Auger electrons of the fragmenting N^+/N^+ channel we reached a resolution of 1.9 a.u. in jet, 0.85 a.u. in the photon beam and 0.75 a.u. in the TOF direction.

The momentum offset due to the initial jet velocity is approximately 10 a.u. This corresponds to a position shift of 14 mm on the detector. Since only a small solid angle of the almost back-to-back emitted ions is detected, the detector had to be shifted upwards in order to maximize the ion/ion coincidence signal. Otherwise in many cases only one ion would have been detected and its partnering, back-to-back emitted, ion would have been lost. The overall acceleration length on the ion side is 83 mm, while the lens is centered around 67 mm. Furthermore, no mesh was used to separate the drift from the acceleration region. This increased the overall detection efficiency by nearly 50%, but also added a bulged field that defocused the ion trajectories. To compensate for this effect, the electrostatic lens had to be a little stronger compared to the case incorporating a mesh. The time focusing geometry was achieved by adding a 642 mm long field-free drift tube.

Figure 1 shows a simulation of the spectrometer used. The simulation was performed using Simion 7.0 for a 130 K precooled N_2 target (corresponding a 10 a.u. offset momentum), a target size of $4 \times 4\,\mathrm{mm}^2$ and ions with 90 a.u. momentum (9 eV KER). A coincidence detection angle of 3.6% of 4π was achieved. It scales linearly with the applied electric field. Ions emerging in the extended target are projected and focused on the detector to a position spread of <0.4 mm and a focus in TOF <5 ns. With respect to the gas jet and photon beam overlap (2 mm in the beam propagation direction and <0.5 mm in the perpendicular directions), we could expect a resolution of 0.1 a.u. in TOF and 0.25 a.u. in the position direction. Taking the momentum uncertainty of the jet temperature (in the expansion direction) into account the simulated and experimentally achieved ion momentum resolution agree satisfactory. The resolution for the Auger electrons calculated from the dissociating channel ($N^+ + N^+$) is a factor 2 worse compared to the non-dissociating channel (N_2^{2+}). This might be due to: (i) nonlinearity effects of the square detector used (local resolution $<100\,\mu$m, but average resolution around 1 mm) and/or (ii) all inhomogeneous field areas in the spectrometer (lenses) are not linear in their properties (focus/defocus stronger in the outer region) and have to be deconvoluted during the analysis. The latter process is absolutely necessary and increases the resolution by a factor of 2–3. It still

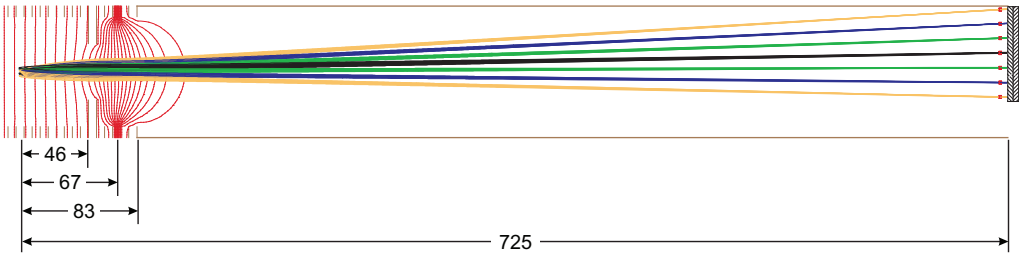

Figure 1. Simulated time and space focusing recoil ion arm of the spectrometer with 10 a.u. offset momentum of the gas jet (corresponding to an N_2 jet at 130 K) and 9 eV KER. The simulated target size is $4 \times 4\,mm^2$ and differently colored trajectories correspond to certain back-to-back emitted ion pairs (black 0/180°, green 5/185°, blue 10/190° and orange 15/195°). Dimensions are given in (mm). Electrons are measured in coincidence with the ions and projected to the left side, but are not shown here.

does not work perfectly and has some room for further improvement (software, spectrometer design and a hexagonal detector with increased linearity).

3. Results

The K-shell photoemission with subsequent Auger decay leads to a wealth of electronically excited states of the N_2^{2+} ion. These states are repulsive and finally lead to two N^+ ions with a KER in the range of 4–20 eV. Correspondingly the Auger energy spectrum is also broad and contributions from different states overlap in energy. By using the information on the angular distribution many of these decay pathways can be unraveled [32, 33]. As outlined in the introduction it is essential to select decay routes where the N_2^{2+} ion is in a state of well-defined symmetry. We have therefore selected events where the kinetic energy release KER is between 8.1 and 9.3 eV only for all the cases discussed below. This corresponds to the $c^1\Delta_g$ and $D^1\Sigma_g^+$ states of N_2^{2+} ion [33]. Thus the final ionic state is selected to be of gerade symmetry. As the neutral initial state is also of gerade parity and the photon absorption results in a change of symmetry, the combined wave functions of the photoelectron and the Auger electron must be of ungerade symmetry. This does not imply that the photoelectron and the Auger electron or the intermediate core hole state of the N_2^+ ion have well-defined symmetry though.

For a selected subset of the data, figure 2 shows the photoelectron angular distribution in the molecular frame, as indicated by the barbells, in the polarization plane of the circularly polarized light. From panels (a) to (d), the excess energy (5, 10, 18 and 56 eV) of the photoelectron, and therefore its wavelength, is varied from 0.26 to 0.08 a.u. Describing the electron emission process in a multiple scattering approach, the angular distributions result from the coherent superposition of all possible paths the electron can take from where its wave is launched. All these pathways are diffracted inside the molecular potential and interfere, leading to richly structured angular distributions. The diffraction term depends on the wavelength and therefore the kinetic energy of the electron. One much discussed aspect of these interferences is the shape resonance around 9 eV electron energy. In this energy range, constructive interference leads to an increase of the photoionization cross section [7, 8] for the creation of a core hole of ungerade character.

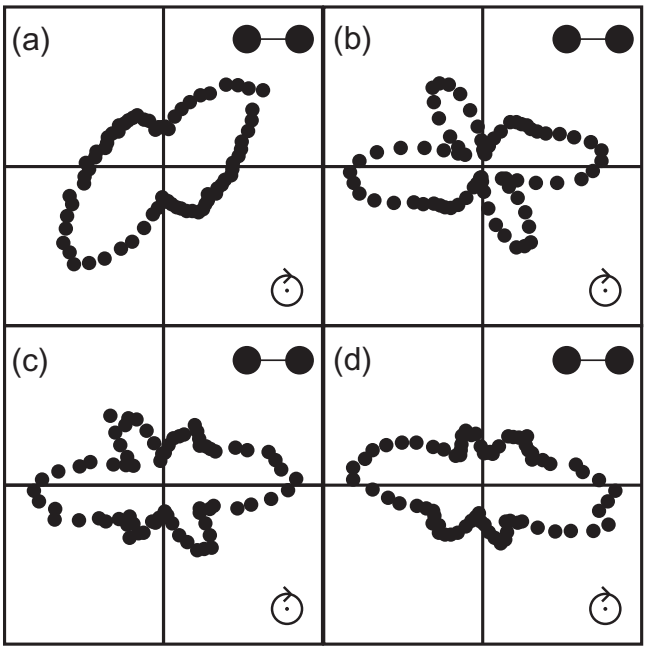

Figure 2. Photoelectron angular distribution integrated over all Auger electron emission angles at (a) 414 eV, (b) 419 eV, (c) 427 eV and (d) 465 eV photon energies.

By changing the photoelectron energies, the Auger electron angular distribution for a given symmetry of the intermediate hole does not change. Since the ratio of the cross section for the creation of a gerade or ungerade core hole in the intermediate state changes across the shape resonance, the overall Auger electron angular distribution changes slightly if integrated over the photoelectron angle. Figure 3 shows this behavior for the four different photon energies. The full lines represent the distribution expected for an optical double slit ($\cos(\vec{k}\cdot\vec{r}/2)$; blue lines) and for an optical double slit with a π phase shifter in one of the slits ($\sin(\vec{k}\cdot\vec{r}/2)$; red lines), where $\vec{k}$ is the photoelectron momentum and $\vec{r}$ the distance of the slits. These simple optical analogues nicely reproduce the position of the maxima and minima. This indicates that the key ingredient of the Auger electron angular distribution is indeed the superposition of two spherical waves emerging from the two centers, as recently demonstrated in [13], as well. The multiple scattering of the outgoing wave at the neighboring center plays a minor role at this high energy of the Auger electron. This is very different for the photoelectrons (see figure 2). They show no reminiscence of a double-slit interference. Their energy is so low that the plane wave approximation that is inherent in the optical analogue fails completely. Their angular distribution is dominantly shaped by the multiple scattering. As shown in [31, 32], there are angular regions of the emitted photoelectrons that almost solely correspond to gerade or ungerade symmetry of the N_2^+ ion core hole state. Thus, by choosing Auger electrons that are in coincidence with the photoelectrons of preselected parity together with our selection of the parity of the N_2^{2+} parity via the KER, we can investigate the Auger electron angular distribution for a fixed symmetry. These Auger electron distributions are shown in figure 4. They exhibit pronounced interference fringes, where maxima and minima are interchanged when we change the symmetry of the corresponding photoelectron (and thus the symmetry of the Auger electron).

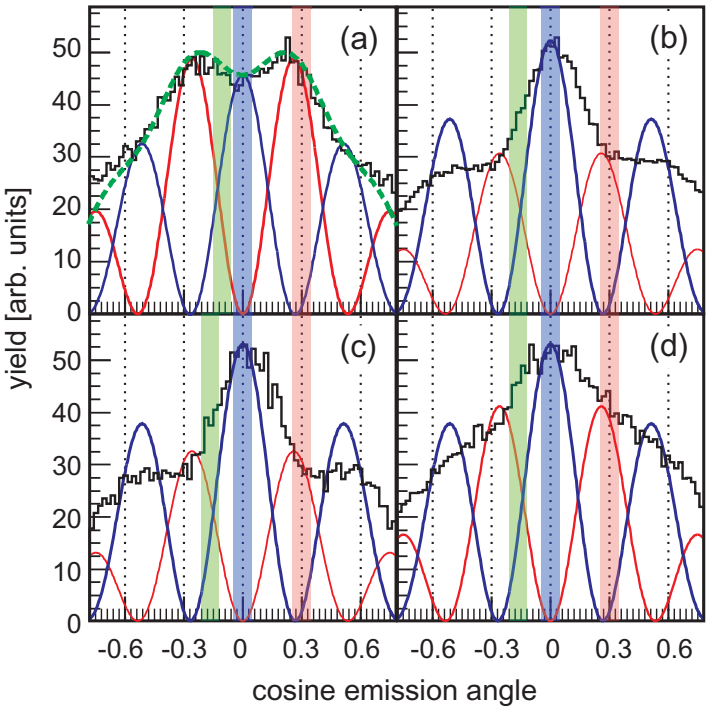

Figure 3. Angular distribution of the Auger electrons at (a) 414 eV, (b) 419 eV, (c) 427 eV and (d) 465 eV photon energies. Solid lines represent theory curves for double slits with a width of $r = 2.2$ Å and an electron of 370 eV: the blue curve for a regular double slit ($\cos(\vec{k} \cdot \vec{r})$) and the red curve with a π phase shifter at one slit ($\sin(\vec{k} \cdot \vec{r})$). (a) The green dashed curve shows the sum of the red and blue curves. The statistical error bars are comparable to the line width.

Of course, the corresponding approach can be used to gather information on the angular distribution of the photoelectron for a given symmetry: figures 5 and 6 show the corresponding gerade or ungerade photoelectron angular distributions for the different photon energies. In order to extract these data from the total photoelectron cross section, we applied gates on the Auger electron angular distributions, as indicated by the blue (gerade) and red (ungerade) shaded areas in figure 3. We observe a strong dependence of the photoelectron angular distribution on the photoelectron wavelength for both parities. The wavelength of these photoelectrons is so long that $\vec{k} \cdot \vec{r}$ is smaller than π. Thus the two-center interference term does not even reach the first interference minimum. Therefore the nodes in the gerade and ungerade photoelectron angular distributions do not stem from any two-center interference. As discussed above they are purely a result of the second type of interference (multiple scattering). It is created by the superposition of the direct (gerade or ungerade) photoelectron wave with the secondary waves created by its multiple scattering in the molecular potential.

Finally, we superimpose the gerade and ungerade photoelectron waves by selecting Auger electron angles of 93–99° or 97–102°. In these intervals, highlighted by the green shaded area in figure 3, the amplitudes of gerade and ungerade Auger electrons are almost equal. For a long time it was believed that such superposition of the gerade and ungerade photoelectron waves has to be done incoherently, i.e. only the emission probabilities have to be added [10, 40–42].

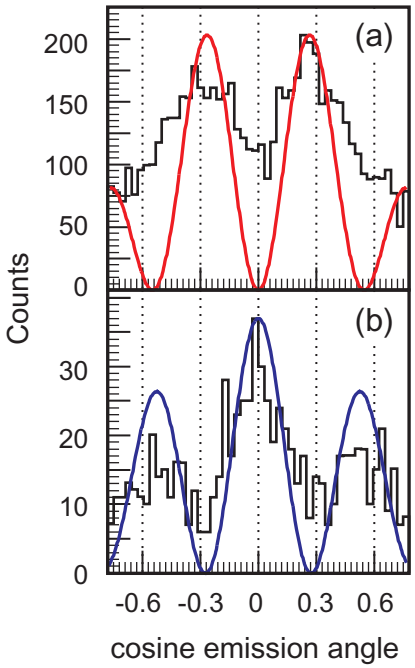

Figure 4. Ungerade (a) and gerade (b) Auger electrons, generated by gating on the photoelectron emission angles (a) 20–65° and (b) 90–100° (at 465 eV photon energy). The solid line represents theory curve for a double slit with a width of $r = 2.2$ Å and an electron of 370 eV, the blue curve (b) for a regular double slit ($\cos(\vec{k}\cdot\vec{r})$) and the red curve (b) with a π-phase shifter at one slit ($\sin(\vec{k}\cdot\vec{r})$). Note that only events with a KER between 8.1 and 9.3 eV are chosen. This corresponds to the $c^1\Delta_g$ and $D^1\Sigma_g^+$ states of N_2^{2+} (see text).

Such incoherent superposition yielded excellent agreement with all available data on photoelectron angular distributions (see, e.g., [10, 40]). This is due to the fact that the cross terms of the amplitudes vanish if one integrates over the Auger electron angular distribution [43]. Only if the Auger electron is measured in coincidence with the photoelectron, the cross terms remain and the interference between gerade and ungerade photoelectron waves becomes visible. In turn this allows us to study the relative phase between the gerade and ungerade photoelectron waves. This is shown in figure 7, where the emission angles of the Auger electrons are selected where the amplitudes of the gerade and ungerade contributions are almost equal. While an incoherent sum would still show a left/right symmetric distribution, the coherent sum from equation (1) breaks this symmetry and promotes the photoelectron in a pure left or right state, which is either the sum or difference of the gerade and ungerade states. As the relative contributions of gerade and ungerade parities vary with photon energy, also the angular region where both parities are almost equally strong changes. To achieve a maximum left/right contrast, the gerade and ungerade parities have to be equally strong. Otherwise one of them would dominate the angular distribution and the left/right symmetry breaking effect would vanish. Therefore it is crucial to select the correct gate on the Auger electron angle; here (b)–(d) are different from (a), where the gerade and ungerade amplitudes contribute similarly (see figure 3). To enhance this point, in figure 7(b) the left inset shows the photoelectron angular distribution with a gate on a different

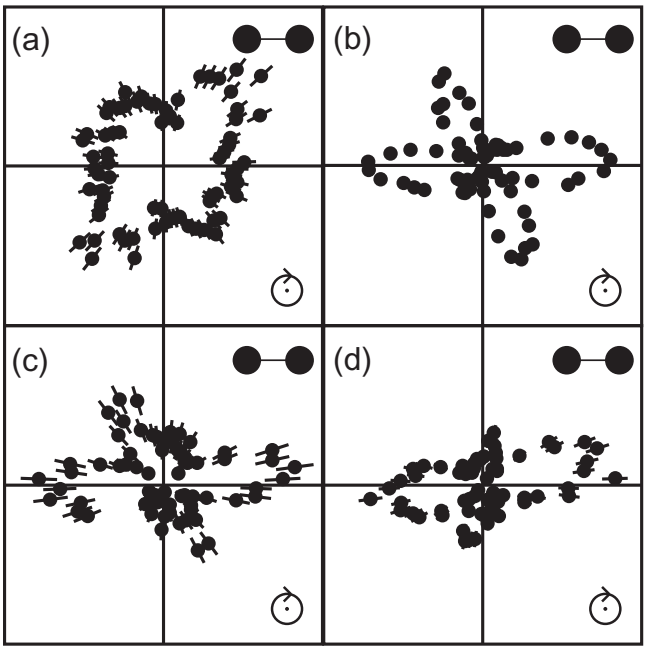

Figure 5. Angular distribution of the gerade photoelectrons (gated on the Auger electron emission angle 87–93°, see the blue shaded area in figure 3) at (a) 414 eV, (b) 419 eV, (c) 427 eV and (d) 465 eV photon energies.

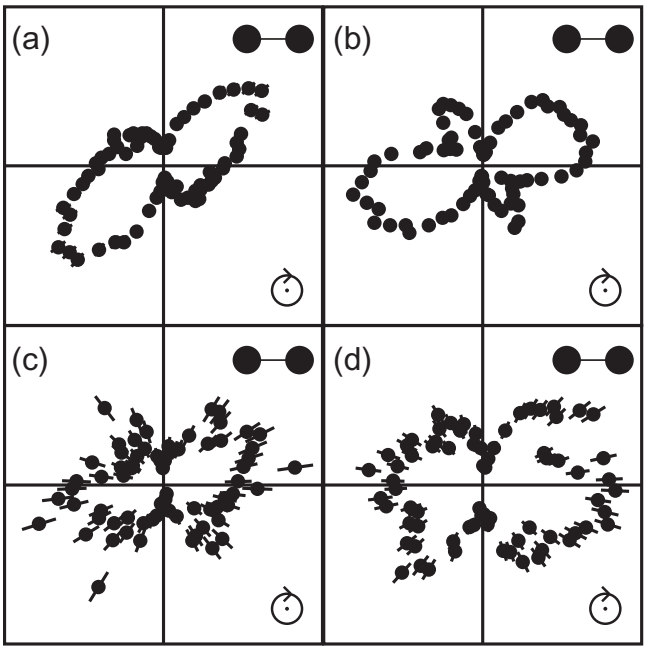

Figure 6. Angular distribution of the ungerade photoelectrons (gated on the Auger electron emission angle 70–75°; see red shaded area in figure 3) at (a) 414 eV, (b) 419 eV, (c) 427 eV and (d) 465 eV photon energies.

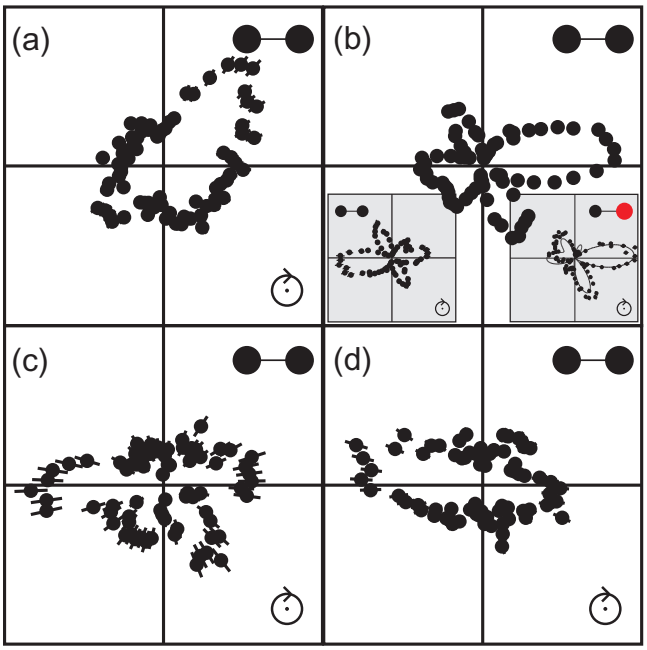

Figure 7. Angular distribution of the 'left' photoelectrons (gated on the Auger electron emission angle: a (93–99°) and b–d (97–102°); see green shaded area in figure 3) at (a) 414 eV, (b) 419 eV, (c) 427 eV and (d) 465 eV photon energies. The left inset in (b) shows a similar photoelectron angular distribution with a gate on the Auger electron emission angle 117–120°. A similar right/left asymmetric pattern can be observed for all photon energies for Auger electron emission angles around 120° (not shown here). The right inset in (b) shows the photoelectron angular distribution for CO.

Auger electron emission angle, where the gerade and ungerade amplitudes contribute again equally. At higher photon energies (b)–(d), on and above the shape resonance, the ungerade parity is stronger compared to the gerade. As a comparison in figure 7(b), the right inset shows the right/left asymmetric photoelectron emission in the by definition localized system of CO after 1s ionization of the carbon atom, i.e. a case where the emission is localized to one site.

4. Conclusion

In conclusion, we have shown that the Auger electron and the photoelectron form an entangled state in the K-shell ionization of a diatomic molecule (N_2). The single-particle basis from which this entangled state is formed is gerade and ungerade (rather than spin-up and -down). Analogous to spin-type Bell states the measurement of the spin component of one particle fixes the spin of the second; in our case a measurement of the parity of one of the electrons fixes the parity of the second one. We select electrons of one parity by choosing a certain angle with respect to the molecular axis where the contribution of this parity maximizes and the opposing parity state emission pattern has a node. We can investigate the interference term between the photoelectron waves of gerade and ungerade parities by selecting Auger electrons at angles where the states of both parities contribute equally. This demonstrated that

the angular distribution of the photoelectron is a result of an interfering gerade or ungerade wave that is multiply scattered in the molecular potential. The angular dependence of the phase of these gerade and ungerade waves changes with electron wavelength. The optical Gedanken-experiment analogue to the presented molecular investigation would be a classical double slit with a wavelength depending on phase shift at one of the slits.

Acknowledgments

We are indebted to K Ueda, L Cederbaum, U Becker and U Hergenhahn for useful discussions. MS thanks the Alexander von Humboldt foundation for financial support. We acknowledge outstanding support from the staff at the Advanced Lights Source, in particular by Hendrik Bluhm and Tolek Tyliszczak. This work was supported by the Deutsche Forschungsgemeinschaft and by the Office of Basic Energy Sciences, Division of Chemical Sciences, US DOE under contract number DE-AC03-76SF00098.

References

[1] Zimmermann B *et al* 2008 Localization and loss of coherence in molecular double-slit experiments *Nature Phys.* **4** 649–55
[2] Rehr J J and Albers R C 2000 Theoretical approaches to x-ray absorption fine structure *Rev. Mod. Phys.* **72** 621–54
[3] Azároff L V 1963 Theory of extended fine structure of x-ray absorption edges *Rev. Mod. Phys.* **35** 1012–21
[4] Bradshaw A M and Woodruff D P 1994 Adsorbate structure determination on surfaces using photoelectron diffraction *Rep. Prog. Phys.* **57** 1029
[5] Landers A L *et al* 2001 *Phys. Rev. Lett.* **87** 013002
[6] Guo F Z, Matsushita T, Daimon H and Matsui F 2007 Circularly polarized x-ray photoelectron diffraction—stereo photograph of atomic arrangement *J. Electron Spectrosc. Relat. Phenom.* **156** 1–9
[7] Dehmer J L and Dill D 1975 *Phys. Rev. Lett.* **35** 213
[8] Shigemasa E, Adachi J, Soejima K, Watanabe N, Yagishita A and Cherepkov N A 1998 *Phys. Rev. Lett.* **80** 1622
[9] Adachi J, Hosaka K, Furuya S, Soejima K, Takahashi M, Yagishita A, Semenov S K and Cherepkov N A 2003 Shape-resonance-enhanced vibrational effects in the angular distributions of c 1s photoelectrons from fixed-in-space CO molecules *Phys. Rev. Lett.* **91** 163001
[10] Jahnke T *et al* 2002 Circular dichroism in k-shell ionization from fixed-in-space CO and N_2 molecules *Phys. Rev. Lett.* **88** 073002
[11] Semenov S K, Cherepkov N A, Jahnke T and Dörner R 2004 Theoretical study of vibrationally resolved photoionization for the C K-shell of CO molecule *J. Phys. B: At. Mol. Opt. Phys.* **37** 1331
[12] Matsumoto M *et al* 2006 Vibrationally resolved photoionization of the $1\sigma_g$ and $1\sigma_u$ shells of N_2 molecule *J. Phys. B: At. Mol. Opt. Phys.* **39** 375
[13] Cherepkov N A *et al* 2010 Auger decay of $1\sigma_g$ and $1\sigma_u$ hole states of the N_2 molecule. II. Young-type interference of Auger electrons and its dependence on internuclear distance *Phys. Rev.* A **82** 023420
[14] Walter M and Briggs J 1999 Photo-double ionization of molecular hydrogen *J. Phys. B: At. Mol. Opt. Phys.* **32** 2487
[15] Kaplan I G and Markin A P 1969 Interference phenomena in photoionization of molecules *Sov. Phys.—Dokl.* **14** 36–9
[16] Cohen H D and Fano U 1966 Interference in the photo-ionization of molecules *Phys. Rev.* **150** 30–3
[17] Akoury D *et al* 2007 A two-electron double slit experiment—interference and entanglement in photo double ionization of H_2 *Science* **319** 949

[18] Kreidi K *et al* 2008 Interference in the collective electron momentum in double photoionization of H_2 *Phys. Rev. Lett.* **100** 133005
[19] Horner D A, Miyabe S, Rescigno T N, McCurdy C W, Morales F and Martín F 2008 Classical two-slit interference effects in double photoionization of molecular hydrogen at high energies *Phys. Rev. Lett.* **101** 183002
[20] Stolterfoht N *et al* 2001 Evidence for interference effects in electron emission from H_2 colliding with 60 MeV/u Kr^{34+} ions *Phys. Rev. Lett.* **87** 0232011–4
[21] Misra D, Kadhane U, Singh Y P, Tribedi L C, Fainstein P D and Richard P 2004 Interference effect in electron emission in heavy ion collisions with H_2 detected by comparison with the measured electron spectrum from atomic hydrogen *Phys. Rev. Lett.* **92** 153201
[22] Misra D *et al* 2009 Two-center double-capture interference in fast $HE^{2+} + H_2$ collisions *Phys. Rev. Lett.* **102** 153201
[23] Chelkowski S and Bandrauk A D 2010 Visualizing electron delocalization, electron–proton correlations, and the Einstein–Podolsky–Rosen paradox during the photodissociation of a diatomic molecule using two ultrashort laser pulses *Phys. Rev.* A **81** 062101
[24] Ciappina M F and Cravero W R 2009 Two center and Coulomb effects in near-threshold ionization of H_2^+ by short laser pulses *J. Mod. Opt.* **56** 11–26
[25] He F, Becker A and Thumm U 2008 Strong-field modulated diffraction effects in the correlated electron-nuclear motion in dissociating H_2^+ *Phys. Rev. Lett.* **101** 213002
[26] Schöffler M *et al* 2008 Photo-double-ionization of H_2: two-center interference and its dependence on the internuclear distance *Phys. Rev.* A **78** 013414
[27] Ehara M *et al* 2006 Symmetry-dependent vibrational excitation in N 1s photoionization of N_2: experiment and theory *J. Chem. Phys.* **124** 124311
[28] Guillemin R, Shigemasa E, Guen K, Le Ceolin D, Miron C, Leclercq N, Morin P and Simon M 2001 *Phys. Rev. Lett.* **87** 203001
[29] Weber Th *et al* 2003 *Phys. Rev. Lett.* **90** 153003
[30] Liu X-J *et al* 2008 Breakdown of the two-step model in *k*-shell photoemission and subsequent decay probed by the molecular-frame photoelectron angular distributions of CO_2 *Phys. Rev. Lett.* **101** 083001
[31] Schöffler M S *et al* 2008 Ultrafast probing of core hole localization in N_2 *Science* **320** 920–3
[32] Cherepkov N A *et al* 2009 Separation of Auger transitions into different repulsive states after *k*-shell photoionization of N_2 molecules *Phys. Rev.* A **80** 051404
[33] Semenov S K *et al* 2010 Auger decay of $1\sigma_g$ and $1\sigma_u$ hole states of the N_2 molecule: disentangling decay routes from coincidence measurements *Phys. Rev.* A **81** 043426
[34] Dörner R, Mergel V, Jagutzki O, Spielberger L, Ullrich J, Moshammer R and Schmidt-Böcking H 2000 Recoil ion momenum spectorscopy—a momenum microscope to view atomic collision dynamics *Phys. Rep.* **330** 96–192
[35] Ullrich J, Moshammer R, Dorn A, Dörner R, Schmidt L Ph H and Schmidt-Böcking H 2003 Recoil-ion and electron momentum spectroscopy: reaction-microscopes *Rep. Prog. Phys.* **66** 1463–545
[36] Jahnke T, Weber T, Osipov T, Landers A L, Jagutzki O, Schmidt L P H, Cocke C L, Prior M H, Schmidt-Böcking H and Dörner R 2004 Multicoincidence studies of photo and Auger electrons from fixed-in-space molecules using the COLTRIMS technique *J. Electron Spectrosc. Relat. Phenom.* **141** 229–38
[37] Jagutzki O, Mergel V, Ullmann-Pfleger K, Spielberger L, Spillmann U, Dörner R and Schmidt-Böcking H 2002 A broad-application microchannel-plate detector system for advanced particle or photon detection tasks: large area imaging, precise multi-hit timing information and high detection rate *Nucl. Instrum. Methods* A **477** 244–9
[38] Moshammer R, Unverzagt M, Schmitt W, Ullrich J and Schmidt-Böcking H 1996 *Nucl. Instrum. Methods* B **108** 425
[39] Dörner R *et al* 1995 *Nucl. Instrum. Methods* B **99** 111
[40] Cherepkov N A, Semenov S K, Hikosaka Y, Ito K, Motoki S and Yagishita A 2000 *Phys. Rev. Lett.* **84** 250

[41] Shigemasa E, Adachi J, Oura M and Yagishita A 1995 Angular distributions of 1sσ photoelectrons from fixed-in-space N_2 molecules *Phys. Rev. Lett.* **74** 359

[42] Dilll D and Wallace S 1978 Molecular-photoelectron angular distributions as a probe of dynamic symmetry breaking *Phys. Rev. Lett.* **41** 1230

[43] Cherepkov N A, Semenov S K and Drner R 2008 Photoelectron–Auger electron angular correlations in photoionization of fixed-in-space molecules *J. Phys.: Conf. Ser.* **141** 012001